Optimizing Distributed Space-Based Networks for Cislunar Space Domain Awareness In the Context of Operational Cost Metrics

Gregory P. Badura[1], Matthew Gilmartin[2], Yuri Shimane[2], Stef Crum[2], Lois Visonneau[2], Christopher R. Valenta[1], Michael Steffens[2], Selcuk Cimtalay[2], Francis Humphrey[2], Mariel Borowitz[2], Brian Gunter[2], John Christian[2], Koki Ho[2]

[1]*Georgia Tech Research Institute,* [2]*Georgia Institute of Technology*

ABSTRACT

Performing Space Domain Awareness (SDA) on the cislunar volume is infeasible with any single Electro-Optical or Infrared (EO/IR) sensor system. This difficulty results from factors such as the vast expanse of cislunar space, the chaotic dynamic conditions, and the time-varying illumination backgrounds across the volume. These complications necessitate the development of collaborative networks of distributed space-based sensors to close coverage gaps of existing Earth-based infrastructure and enable persistent cislunar SDA.

We show progress on optimizing the distributed sensor optimization problem from the lens of not only the performance of technologies but also operational constraints that are unique to the Cislunar domain. Models representing both of these factors have been assembled into software packages to enable a Model-Based Systems Engineering (MBSE) analysis of the problem. In order to perform optimization studies across the library of potential models, we have further developed a rapidly configurable Multi-Disciplinary Analysis and Optimization (MDAO) modeling framework. The MDAO framework uses object-oriented programming techniques to standardize model interfaces and allow them to be integrated into a unified optimization environment that is extended from NASA's OpenMDAO package. At the optimization stage, this MDAO system leverages genetic algorithms to produce the optimal choice of technologies and designs with respect to desired operational performance metrics. The end result is a modular software package that can be used to execute optimizations across a range of present and future cislunar technologies and designs.

We provide an overview of how the metrics for sensor detection performance and orbit maintenance costs can be integrated into a library of optimization metrics. These metrics were used to assess the performance of distributed sensor networks consisting of observers spanning the cislunar space. Sensor detection performance is quantified by the percentage of the coverage over time, whereas the maintenance costs are quantified by orbit instability and navigation uncertainty. These cost metrics are used to optimize the SDA architecture while considering the operational challenges of deploying and maintaining distributed sensors within the chaotic cislunar volume. We present our results in the form of a Pareto front of non-dominated solutions to each of the specified performance metrics and detail changes in how architecture optimization changes once our operational cost metrics are considered.

1. INTRODUCTION

Recent market research surveys indicate that upwards of 250 lunar missions with economic costs totaling $100 Billion dollars are expected by the year 2030 [1]. The increased amount of lunar-bound traffic necessitates the development of Space Domain Awareness (SDA) networks to monitor satellite motions in the Beyond Geostationary (xGEO) region. While there are currently many commercial, national, and international assets available to surveil the near-Earth regimes of Low-Earth Orbit (LEO), Medium Earth Orbit (MEO), and Geostationary Orbit (GEO), these existing surveillance systems are not readily extendable to the cislunar domain [2].

One of the primary reasons for this is that lunar gravity cannot be neglected or treated as a perturbation to a dynamic model for cislunar object tracking as in the case of dynamic models of near-Earth orbiting satellites [3]. Cislunar satellites are affected by both the Earth and the Moon's gravitational forces; their motion must therefore be modeled using three-body dynamics which are well known to be chaotic even for simplified approximations [4]. An additional complication to performing tasks such as Initial Orbit Determination (IOD) on satellites in the cislunar region from

near-Earth infrastructure is that objects in cislunar space can appear to move very slowly from the perspective of an observer based on the Earth's surface or even orbiting the Earth; this means that there may be insufficient geometric diversity for generating reliable IOD position and velocity estimates of the cislunar satellite's motion [3]. Finally, from the perspective of electro-optical sensor tasking, the vast volume of the cislunar regions poses challenges for detecting object signatures, let alone consistently tracking the objects [5]. The Earth-Moon distance is roughly $10\times$ greater than GEO altitude and certain low-energy transfers can have apogees extending to approximately 1.5 million kilometers, which is roughly five times the Earth-Moon distance [2, 5]. This represents a nearly $1000\times$ increase in coverage volume relative to the volume extending out to GEO orbit that the current United States Space Force (USSF) SDA infrastructure is tasked with monitoring [2]. In addition to collecting sufficient numbers of photons for detection of assets, certain viewing geometries can pose substantial challenges for detection of lunar-bound assets. In particular, the Air Force Research Laboratory (AFRL) has termed a conical section of approximately 30° surrounding the Earth-Moon direction as the "cone of shame" due to the inability to detect dim targets against the relatively bright backdrop of the lunar surface [6]. The need to decrease sensor standoff ranges and increase the geometric diversity of electro-optical observations makes distributed space-based constellations a desirable solution to overcome the limitations of near-Earth and Earth-based SDA infrastructure.

There have been several recent studies that focused on optimizing the surveillance of the cislunar volume via distributed space-based sensors. Many of these studies focus on optimizing some variation of the percentage of a search-volume that is considered "visible" to the architecture over time [3, 5, 7, 8, 9, 10, 11]. While the definition of "visibility" varies across these studies, the ultimate findings of all of these studies indicate that there is no single cislunar orbit family that solves the challenge of continuously detecting objects in the cislunar volume over extended periods of time. These results indicate that a diverse array of space-based assets must be deployed in order to provide geometric and spatial diversity to overcome the challenges of surveilling the cislunar volume using electro-optical means [3, 11]. These studies, however, ultimately fall short in that they do not consider cost factors that could potentially render orbital families with high detection performance infeasible from an operational perspective. In this paper, we propose several novel optimization metrics that capture these cost factors and combine them into a cost function that considers not only detection performance but also the operational challenges of performing station keeping and maintaining inertial positioning of a surveillance asset.

This paper is organized as follows: In Section 2, we introduce the modeling of motions in the Earth-Moon system under three body conventions and cover the concept of equilibrium orbits that are desirable for long-term cislunar surveillance. In Section 3, we introduce several existing and new optimization metrics, which span from considering percentage visibility to new operational cost factors for station keeping and inertial navigation. In Section 4, we introduce the cost functions over which space-based constellations will be optimized, and the Multi-Disciplinary Analysis Optimization (MDAO) framework that is leveraged to optimize said cost functions over configurable design reference missions. In Section 5, we introduce the design reference mission for this study that optimizes over the observability of targets spanning a conical volume centered on the Earth-Moon direction in the rotating Earth-Moon frame. Finally, in Section 6 we present results on the optimal space-based architectures in the context of two different cost functions: (1) the percentage search-volume visible to the architecture over time, and (2) a combined metric of the percentage search-volume visible to the architecture over time and the costs due to orbit instability and optical navigation uncertainty.

2. CISLUNAR DYNAMICS

Motion within the Earth-Moon system is typically approximated by using Circular Restricted Three-Body Problem (CR3BP) dynamics. Under the dynamics of the CR3BP, a spacecraft of negligible mass undergoes motion due to the gravitational influence of two primary bodies (Moon and Earth) that are approximated as point masses [12]. In order to simplify the equations of motion, the position and velocity of the spacecraft are expressed in terms of a non-inertial coordinate system that rotates with an angular velocity of magnitude equal to the rate of rotation of the primary masses moving in circular orbits about their barycenter [3]. These approximations are typically highly successful for modeling the motion of spacecraft traversing the cislunar domain due to the relatively low eccentricity of the Moon's orbit and the small effect of the Sun's gravitational effect, especially in the vicinity of the Earth or Moon [4].

In terms of the non-inertial rotating frame, the acceleration of a spacecraft at position $\mathbf{r}_D$ undergoing gravitational

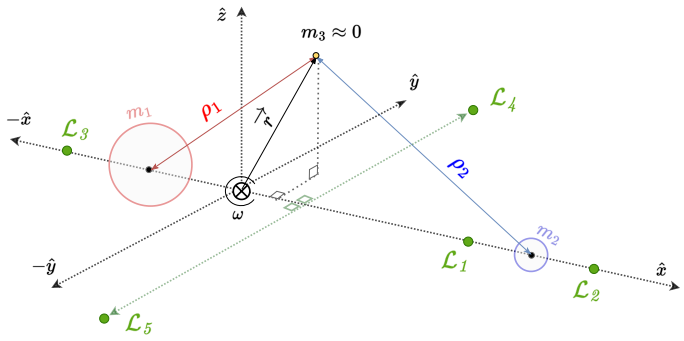

Fig. 1: Diagram of the rotating frame of the Circular Restricted Three-Body Problem (CR3BP). A spacecraft of negligible mass ($m_3 \approx 0$) at non-dimensional position ($\mathbf{r}$) is acted upon by two primary masses oriented along the x-axis of the rotating frame. Approximate positions of equilibrium points ($L1$-$L5$) are shown in green for locations where the gradient of the pseudopotential (∇U) approaches a value of zero [3, 11].

force by a large primary mass at location $\mathbf{r}_{1_D}$ and a smaller primary mass located at location $\mathbf{r}_{2_D}$ is written as [13, 12]:

$$\ddot{\mathbf{r}}_D = -\frac{Gm_1}{|\mathbf{r}_D - \mathbf{r}_{1_D}|}\begin{bmatrix} x_D + \frac{m_2}{m_1+m_2}|\mathbf{r}_{1_D} - \mathbf{r}_{2_D}| \\ y_D \\ z_D \end{bmatrix} - \frac{Gm_2}{|\mathbf{r}_D - \mathbf{r}_{2_D}|}\begin{bmatrix} x_D - \frac{m_1}{m_1+m_2}|\mathbf{r}_{1_D} - \mathbf{r}_{2_D}| \\ y_D \\ z_D \end{bmatrix} + 2\omega\begin{bmatrix} \dot{y_D} \\ -\dot{x_D} \\ 0 \end{bmatrix} + \omega^2\begin{bmatrix} \dot{x_D} \\ \dot{y_D} \\ 0 \end{bmatrix}, \quad (1)$$

where G is the gravitational constant, m_1 and m_2 (with $m_1 \geq m_2$) are the masses of the two primary bodies, and ω is the magnitude with which the rotating frame spins about the z-axis with angular velocity $\vec{\omega} = [0, 0, \omega]^T$ [13, 3]. From this equation, we can see that the two primary masses are oriented along the x-axis of the rotating frame, with the geometry outlined in Figure 1.

The subscript D in Equation 1 denotes that the units are dimensionalized. This means that the units are expressed according to *SI* unit conventions. According to standard astrodynamics conventions, the state vector components of spacecraft are nearly always non-dimensionalized when propagating motion under the CR3BP [13, 12]. In order to generate non-dimensional positions, all position vectors are therefore scaled by a Distance Unit (DU) equal to the distance in between the primary masses given by: $DU = |\mathbf{r}_{1_D} - \mathbf{r}_{2_D}| \approx 384{,}400$ km. Similarly, the masses of the primary bodies are scaled by 1 Mass Unit (MU) given by: $MU = m_1 + m_2$. This introduces a mass ratio $\mu = m_2/(m_1+m_2) \approx 0.012277471$ that is used to describe non-dimensionalized masses of the two primary bodies. Finally, the *SI* times are scaled by a Time Unit (TU) that is given by: $TU = 1/\omega = \sqrt{\frac{|\mathbf{r}_{1_D} - \mathbf{r}_{2_D}|^3}{G(m_1+m_2)}} \approx 4.348$ days. [3, 12]. After performing this non-dimensionalization, the equation of motion in the rotating frame take on the simpler form of [3]:

$$\ddot{\mathbf{r}} = -\frac{1-\mu}{{\rho_1}^3}\begin{bmatrix} x+\mu \\ y \\ z \end{bmatrix} - \frac{\mu}{{\rho_2}^3}\begin{bmatrix} x-1+\mu \\ y \\ z \end{bmatrix} + 2\begin{bmatrix} \dot{y} \\ -\dot{x} \\ 0 \end{bmatrix} + \begin{bmatrix} \ddot{x} \\ \ddot{y} \\ 0 \end{bmatrix}, \quad (2)$$

where the subscript D has been dropped to signify the equation of motion are non-dimensionalized, and ρ_1 and ρ_2 denote the non-dimensional distances from the spacecraft to the large and small primary bodies, respectively. For the remainder of the paper, we will assume that all position and velocity vectors are non-dimensional unless explicitly stated otherwise.

The form of the non-dimensional acceleration of Equation 2 allows for the expression of CR3BP dynamics in terms of a psuedopotential (U) [5]:

$$U = \frac{x^2+y^2}{2} + \frac{1-\mu}{\rho_1} + \frac{\mu}{\rho_2} \quad (3)$$

$$\frac{\partial U}{\partial x} = \ddot{x} - 2\dot{y} \quad (4)$$

$$\frac{\partial U}{\partial y} = \ddot{y} + 2\dot{x} \quad (5)$$

$$\frac{\partial U}{\partial z} = \ddot{z} \tag{6}$$

The pseudopotential U and it's partial derivatives allow for exploration of equilibrium points (also known as libration points) of the Earth-Moon system as described under CR3BP dynamics [3]. At such equilibrium points, the gravitational forces acting on a spacecraft are balanced due to the gradient of the psuedopotential (∇U) approaching a value of zero [3, 14]. Orbits that are centered on such equilibrium points are attractive to consider because they allow for stable periodic orbits within the chaotic CR3BP system at potentially minimal fuel cost [13, 12]. As we will discuss in Section 3.2, however, the stability (and therefore station-keeping fuel cost) can vary substantially both within orbital families and across different libration point orbits.

The topic of equilibrium points of the CR3BP are discussed in great detail in the work of Fowler and Paley [3], and will therefore only be briefly discussed here. The first three libration points (denoted $L1$. $L2$, and $L3$) lie along the x-axis of the rotating frame of the CR3BP system and can be solved for by setting $\partial U/\partial z = \partial U/\partial x = 0$. This leads to the following solution for the locations of these points in the rotating frame in terms of the spacecraft coordinates [3]:

$$\mathbf{r}_{L1} = ((1-\mu) - \rho_2, 0, 0) \tag{7}$$

$$\mathbf{r}_{L2} = (\rho_2 + (1-\mu), 0, 0) \tag{8}$$

$$\mathbf{r}_{L3} = (-\rho_1 - \mu, 0, 0) \tag{9}$$

The remaining two main libration points (termed $L4$ and $L5$) are found by computing the points at which the distances primaries to the spacecraft are equal (i.e. $\rho_1 = \rho_2 = 1$). The solution to $\partial U/\partial \rho_1 = \partial U/\partial \rho_2 = 0$ at these points shows that the $L4$ and $L5$ points form equilateral triangles with respect to the two primary masses [3]. These points therefore have the following coordinates in the rotating non-dimensional frame:

$$\mathbf{r}_{L4} = \left(\left(\frac{1}{2}\right) - \mu, -\frac{\sqrt{3}}{2}, 0\right) \tag{10}$$

$$\mathbf{r}_{L5} = \left(\left(\frac{1}{2}\right) - \mu, +\frac{\sqrt{3}}{2}, 0\right) \tag{11}$$

From Equations 7-11, a few observations can be made regarding potentially useful equilibrium points for cislunar surveillance. One is that the $L3$ point is located on the farther side of the larger primary mass (i.e. the Earth) with respect to the smaller primary mass (i.e. the Moon), rendering it of limited interest for monitoring major lunar-bound traffic. The other is that the $L4$ and $L5$ points are symmetric with respect to the x-axis of the rotating frame, meaning that they provide similar observability for monitoring lunar-bound traffic traveling in the $+x$ direction of the rotating frame. For these reasons, our study will only consider the surveillance capability of a select set of orbits centered about the $L1$, $L2$, and $L4$ equilibrium points, with the specific orbital families presented later on in Table 1.

In this study, the CR3BP equations of motion defined by Equations 4-6 are propagated over non-dimensional time via the State Transition Matrix (STM) denoted as Φ. The STM is defined according to the following initial value problem:

$$\begin{cases} \dot{\Phi}(t) = \mathbf{A}(\mathbf{x}(t)) \\ \Phi(t) = \mathbf{I}_{6\times 6} \end{cases} \tag{12}$$

where $\mathbf{A}$ is the Jacobian of the CR3BP and $\mathbf{x}(t)$ is the state vector consisting of the position and velocity of the spacecraft at a given moment of time (t) [5].

3. CISLUNAR SURVEILLANCE METRICS

In this section, we present our proposed performance and cost metrics for optimizing the cislunar surveillance problem. In Section 3.1, we present a metric that quantifies the the percentage of the search-volume visible to the architecture over time. Various forms of this metric have been utilized in SDA studies for optimizing the cislunar surveillance problem [8, 3, 11, 5]. While the percentage search-volume metric has been useful for optimizing factors such as stand-off distances and phasing of cislunar satellites, it does not consider operational costs of maintaining a constellation. Therefore, in Sections 3.2-3.3 we present metrics that quantify the costs of orbit instability and navigation uncertainty. These additional metrics allow us to quantify the operational challenges of maintaining distributed sensors within the chaotic cislunar volume, as will be presented in Section 4.1.

3.1 Target Detectability Metric

In order for a space object to be "visible" to an electro-optical telescope, the space object must be sufficiently bright [11] and the telescope aperture must be adequately sized to collect a sufficient number of target photons to enable detection [15]. To capture both of these considerations, our performance metric for target detectability is adopted from previous work by Vendl and Holzinger in which they optimized the fraction of time for which a space object's apparent magnitude was higher than a sensor's cutoff visual magnitude [11]. In this paper we refer to this metric as the percentage of the search-volume visible to the architecture over time, and note that it is the community standard for optimizing cislunar surveillance networks [8, 3, 11, 5].

Vendl and Holzinger's metric treats the target as a spherical satellite of diameter d_T that reflects incident radiance with specular reflectance (ρ_s) and Lambertian reflectance (ρ_d). This shape approximation leads to a closed-form solution of the reflected radiance [16], and consequently allows for the apparent magnitude of the target of a target at location $\mathbf{r}$ being observed by a telescope at location $\mathbf{o}$ to be computed as [11]:

$$m_T(t) = m_S - 2.5\log_{10}\left(\frac{{d_T}^2}{|\mathbf{r}(t)-\mathbf{o}(t)|^2}\left[\frac{\rho_s}{4}+\rho_d p_d(\varphi(t))\right]\right), \tag{13}$$

where $m_S = -26.74$ is the apparent magnitude of the Sun, and φ is the solar phase angle defined as a function of the Sun's location ($\mathbf{s}$) relative to the target and observer locations as [11]:

$$\varphi(t) = \arccos\left(\frac{(\mathbf{o}(t)-\mathbf{r}(t))\cdot(\mathbf{s}(t)-\mathbf{r}(t))}{|\mathbf{o}(t)-\mathbf{r}(t)||\mathbf{s}(t)-\mathbf{r}(t)|}\right), \tag{14}$$

and $p_d(\varphi(t))$ is a closed form solution for a scattering function that defines how a diffusely reflecting sphere scatters incident radiance as a function of solar phase angle [11]:

$$p_d(\varphi(t)) = (2/3\pi)\left(\sin(\varphi(t)) + (\pi-\varphi(t))\cos(\varphi(t))\right) \tag{15}$$

Based on our goal of minimizing the apparent magnitude of the target (m_T), a few observations can be drawn on constellations that will lead to the optimal target-solar-observer geometry at an instantaneous moment of time. From the factor $|\mathbf{r}(t)-\mathbf{o}(t)|^{-2}$ in Equation 13, we can see that minimizing m_T requires the cislunar surveillance asset to continuously maintain low standoff distances from the target. From Equation 15, we can see that minimizing m_T also requires that the cislunar surveillance telescope be phased with respect to the sun such that the observer maintains low solar phase angles with respect to the target's position. These deductions provide guidelines on how we can minimize the apparent magnitude of a target at an instantaneous moment of time. However, we truly desire to know how well a given surveillance asset can maintain custody of a cislunar target over extended durations of time.

Accordingly, Vendl and Holzinger suggested that the apparent magnitude of a target be evaluated over all time steps of the simulation duration to generate a Cumulative Distribution Function (CDF) of target apparent magnitudes from the perspective of an observer's trajectory [11, 5]. After generating this CDF, a cutoff visual magnitude (m_{co}) is used to evaluate the target's apparent magnitude against the limiting visual magnitude of a deployed telescope's optical capabilities [15]. The visibility performance metric of a single target is then considered as the target apparent magnitude in the CDF that meets a requirement that for α-percent of the simulation time steps the target apparent magnitude is greater than the cutoff apparent magnitude, denoted as $M_T(\alpha)$ [11]. Using this framework, the target is deemed visible for the duration of the mission in the context of the telescope's limiting magnitude (m_{co}) and a desired percentage time of custody (α) if it satisfies the equation [5]:

$$M_T(\alpha) \leq m_{co} \tag{16}$$

A diagram outlining the concepts of this metric is shown in Figure 2. In our study, the visibility performance metric used in the optimization framework is defined as the percentage of the total distributed targets (Γ_v) in the cislunar volume that are visible for the mission duration according to Equation 16. For clarify, our approach for computing the Γ_v factor follows from Algorithm 1 of Visonneau et al's optimization study [5].

3.2 Stability Cost Metrics

For a given orbit about an equilibrium point, a stability index for this orbit can be computed by evaluating the eigenvalues of its monodromy matrix. The monodromy matrix ($\Phi(P)$) corresponds to the STM evaluated after propagation

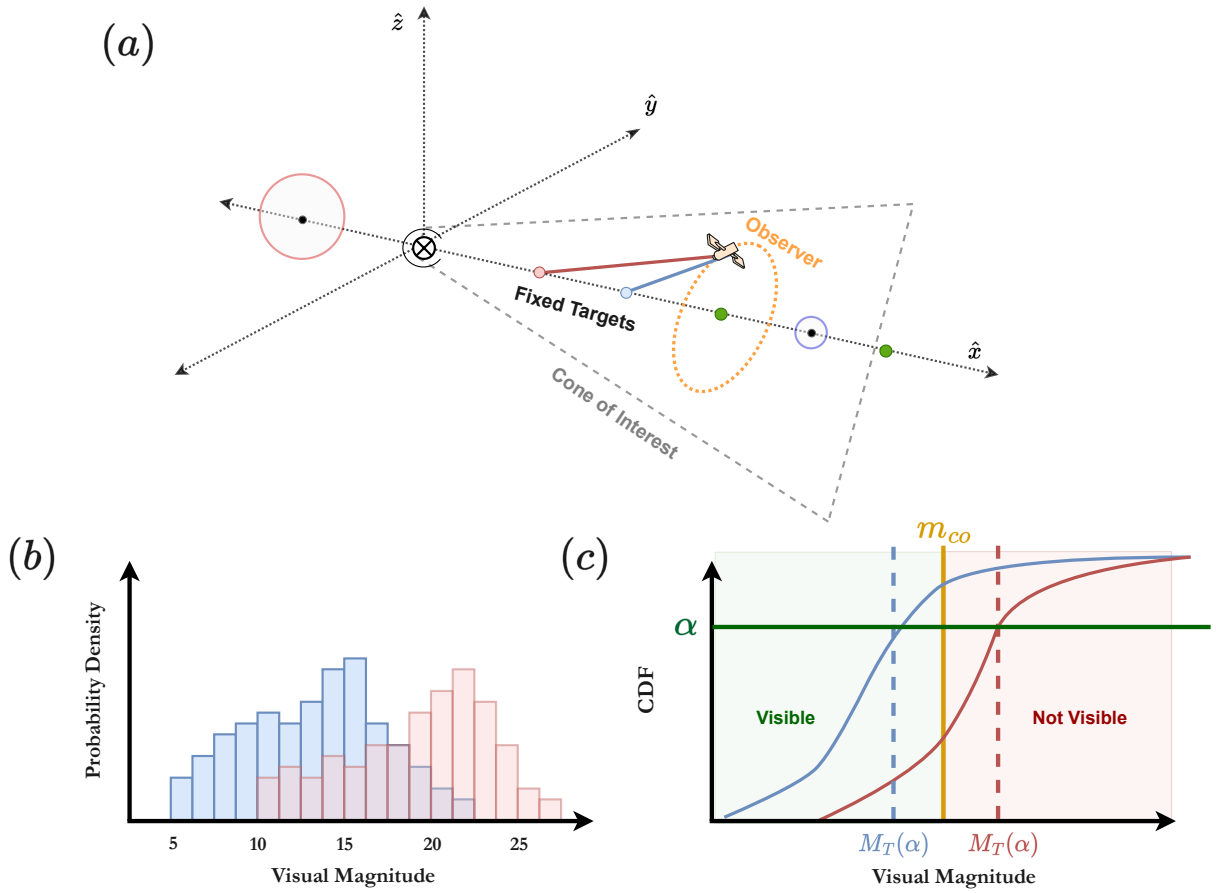

Fig. 2: A diagram outlining the concepts of Vendl and Holzinger's visibility metric [11]: (a) An candidate observer monitoring fixed targets within a volume of interest captures measurements in the form of visual magnitude; (b) the time history of visual magnitude measurements for each target is converted into a Probability Density Function (PDF); (c) the PDF is converted into a Cumulative Density Function (CDF) and the percentage level necessary for successful custody over the time of simulation (α) is used to derive signature $M_T(\alpha)$ that represents the percentage of time that the object is under custody for α% of the time.

of the spacecraft for it's period (P) [5]. The eigenvalues of the monodromy matrix have several interesting properties, including: (1) appearing in reciprocal pairs, and (2) one pair of eigenvalues always being equal to unity due to the periodicity of the orbit [17]. Excluding the trivial pair, the largest eigenvalue of the monodromy matrix (λ_{max}) may used to compute a single metric that describes the stability of the corresponding orbit [5]:

$$\sigma = \frac{1}{2}\left(\lambda_{max} + \frac{1}{\lambda_{max}}\right) \tag{17}$$

It has been shown that a larger value of the stability value of the stability index (σ) is correlated with a faster departure from the reference [17].

3.3 Navigation Performance Metric

Achieving superior inertial navigation performance is critical to ensure that cislunar surveillance activities such as orbit determination and sensor tasking can be accomplished effectively. Studies have shown that uncertainty in an observer's position can flow downstream into cislunar orbit determination solutions [18], that precise navigation estimates are required for planning stationkeeping maneuvers [19], and that certain equilibrium point orbits require more precise positioning and velocity knowledge in order to maintain periodicity of the orbit [20]. For these reasons, the performance of planned navigation algorithms is important to consider when optimizing a cislunar surveillance network.

Typically, the performance of navigation algorithms is assessed by via the output of Linear Covariance (LinCov) approaches or Monte-Carlo simulations of filtering algorithms. While these are proven methods, the computational expense of carrying out tens to hundreds of randomized runs in a MDAO optimization routine is infeasible. These complications necessitate the use of numerical methods that can provide a scalar metric of navigation performance that can be computed on the fly during an MDAO run. We utilize the observability gramian that measures the sensitivity of a chosen navigation algorithm output to the initial conditions of the cisunar surveillance satellite for this purpose [3, 21]. The local observability gramian for a given dynamical system is defined as [21]:

$$P(\mathbf{x}^0) = \int_{t_0}^{\Delta T} \Phi^T(t)\mathbf{H}^T(t)\mathbf{H}(t)\Phi(t)dt \ , \tag{18}$$

where $\mathbf{x}^0$ is the initial state vector, Φ is the fundamental matrix describing the system linear dynamics, and $\mathbf{H}$ is the measurement Jacobian for the output of the navigation algorithm [3]. Computing the observability gramian is computationally expensive for cislunar systems because it requires calculation of the matrix Φ that is dependent on the instantaneous position and velocity of a cislunar asset [22]. A less computationally expensive mode of computing the local observability gramian was therefore suggested in [21]. The (i, j) components of this approximated $(N \times N)$ local observability gramian are given for an N-dimensional state vector by [21]:

$$P^*(\mathbf{x}^0)_{i,j} = \left(\frac{1}{4\delta^2}\right) \int_{t_0}^{\Delta T} \left(\mathbf{y}^{+i}(t) - \mathbf{y}^{-i}(t)\right)^T \left(\mathbf{y}^{+j}(t) - \mathbf{y}^{-j}(t)\right) dt \ , \tag{19}$$

In Equation 19, $\mathbf{y}^{\pm k}(t)$ is the output at time t resulting from an initial state vector that has been perturbed according to $\mathbf{x}^{\pm k} = \mathbf{x}^0 \pm \delta\mathbf{e}^k$, where $\delta > 0$ is a small displacement and $\mathbf{e}^k$ for $k \in [1, ..., n]$ is the k^{th} unit vector in $\mathscr{R}^n$ [3]. The gramian of Equation 19 is faster and more repeatable to compute than the form in Equation 18 because it only requires the ability to simulate the observed dynamical system, which can easily be accomplished with first-order Ordinary Differential Equation (ODE) solvers [5, 9]. In order to assess the degree of observability of the initial state vector $(\mathbf{x}^0)$ from a series of navigation outputs, the condition number of $P^*(\mathbf{x}^0)$ is calculated [3]. The condition number for a matrix is defined as the ratio of the largest local singular value to the smallest. Intuitively, a large condition number indicates that the problem is ill-conditioned because the output resulting from a small change in the initial state in one direction substantially outweighs the effect on the output due to a change in another direction [21]. Therefore, in our optimization routine we seek to minimize the condition number of Equation 19 because this means that the cislunar orbit corresponding to the initial state vector has more stable navigation performance with respect to a perturbation in initial position and velocity.

For this study, we assume that cislunar assets will be performing navigation via Optical Navigation (OPNAV) of the apparent lunar horizon. Historical modes of performing horizon-based OPNAV have used the iterative limb-scanning technique pioneered during the Voyager mission. This method is known to sometimes produce biased results, an effect that can be largely removed using the Christian-Robinson algorithm [23, 24], which is now briefly summarized. The interested reader can refer to the derivation in [23] for the full details.

The goal of the Christian-Robinson OPNAV algorithm is to solve for the center of the celestial body relative to the camera frame $(\mathbf{r}_C)$. The algorithm skips the intermediate conic fit step by factoring the celestial body's symmetric shape matrix $(\mathbf{A}_C)$ into the form $\mathbf{A}_C = \mathbf{B}^T\mathbf{B}$. Carrying out this factorization allows for the celestial body position vector to be transformed via $\mathbf{r}'_C = \mathbf{B}\mathbf{r}_C$. A diagram of this concept and the line-of-sight geometry for a space-based camera is shown in Figure 3. By solving for the conic-fit of the celestial body using the transformed vector $\mathbf{r}'_C$, the problem is re-framed into a simpler form in which navigation is carried out by tracking the horizon of a unit sphere [24]. The Christian-Robinson algorithm therefore translates the problem of horizon based OPNAV into the problem of solving for the vector $\mathbf{r}'_C$. A derivation shows this vector can be related to line-of-sight vectors targeting the center of the celestial body $(\mathbf{r}_C)$ and detected horizon points along the surface of the celestial body (ε_C) via [23]:

$$\mathbf{r}'_C = \left(\frac{1}{\cos^2\phi'} - 1\right)^{-\frac{1}{2}} \mathbf{n}' \ , \tag{20}$$

$$\cos\phi' = \frac{(\mathbf{B}\varepsilon_C)^T(\mathbf{B}\mathbf{r}_C)}{||\mathbf{B}\varepsilon_C||\ ||\mathbf{B}\mathbf{r}_C||} \ , \tag{21}$$

$$\mathbf{n}' = \left(\frac{1}{\cos\phi'}\right) \frac{\mathbf{B}\mathbf{r}_C}{||\mathbf{B}\mathbf{r}_C||} \ , \tag{22}$$

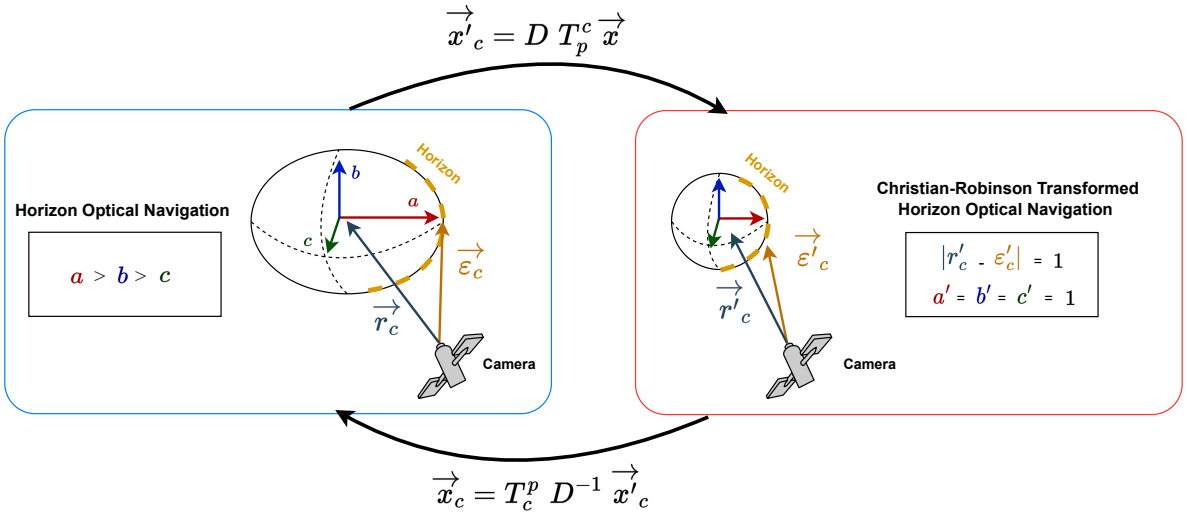

Fig. 3: Diagram of the transform of the Christian-Robinson algorithm being applied to a horizon-based optical navigation problem. An invertible transform ($B = T_p^c D$) is applied to camera line of sight vectors targeting the center ($\mathbf{r}_C$) and horizon points ($\boldsymbol{\varepsilon}_C$) of a planetary body. This transform converts the optical navigation problem from one focused on a celestial body with principal axis dimensions (a, b, c) to one targeting a celestial body with unit and equal principal axis dimensions ($a' = b' = c' = 1$) [23].

$$\mathbf{B} = \mathbf{D}\, \mathbf{T}_P^C\,, \tag{23}$$

where $\mathbf{n}'$ is a vector that is in the direction of $\mathbf{r}'_C$ with a magnitude that is functionally related to the distance between the camera and the celestial body center, $\mathbf{T}_P^C$ is the known attitude matrix that transforms a vector expressed in the camera frame to that same vector expressed in the celestial body frame, and $\mathbf{D} = \text{diag}(1/a, 1/b, 1/c)$ for a celestial body with principal axis dimensions (a, b, c) [24]. While not explicitly stated for simplicity, the body vectors in the camera frame ($\mathbf{r}_C$, $\boldsymbol{\varepsilon}_C$) and the attitude transformation matrix ($\mathbf{T}_P^C$) are both a function of time t for a space-based asset that is traversing the cislunar volume. The computed vector $\mathbf{r}'_C(t)$ serves as the navigation output (i.e. $\mathbf{y}(t)$) that is used to represent our dynamical system in Equation 19. Therefore, the condition number for $P^*(\mathbf{x}^0)$ quantifies the observability of the initial cislunar state vector given a series of lunar horizon OPNAV measurements obtained by a cislunar surveillance asset in our optimization study.

An important distinction between our implementation and the Christian-Robinson algorithm is that in the Christian-Robinson algorithm the vector $\mathbf{n}'$ is estimated via least squares solution across multiple detected horizon points from an image of a celestial body [23]. Because our metric calculation does not rely on simulated imagery of horizon points, we compute the vector $\mathbf{n}'$ directly from geometry and add a zero-mean Gaussian error with standard deviation $\sigma_{HL} = 0.07$ pixels to model the effect of sub-pixel horizon localization on the derived solution of $\mathbf{n}'$ [25].

4. OPTIMIZATION OF DISTRIBUTED CISLUNAR SURVEILLANCE NETWORKS

The metrics that were introduced in Section 3 provide the means to assess the ability of a space-based surveillance asset to both detect target assets and maintain orbital stability over time. We combine these metrics into two different multi-objective optimization function formulations in this paper in order to assess the difference in network design architectures when considering operational cost factors versus when solely considering detection capability. We then introduce the Multi-Disciplinary Analysis and Optimization (MDAO) framework that is used to minimize these two different cost functions via evolutionary optimization techniques and generate the optimal surveillance network for a design reference mission.

4.1 Multi-Objective Cost Functions

The standard approach that is currently utilized in the SDA community for optimizing distributed cislunar architectures is to maximize the the percentage of a volume of interest that is considered to be “visible” to the candidate network

architecture over the extended period of surveillance [3, 5, 8, 11]. The visibility metric normally varies by study, with some studies considering it as a probability of detection [8] and others considering it as the apparent magnitude [5, 11]. Both of these metrics essentially encapsulate how the combined effects of target-to-observer standoff distance and solar phase angle geometry influence the number of photons that will be incident onto an asset's telescope aperture [5]. Our approach for quantifying the detection capability of a surveillance asset adopts the apparent magnitude definition of Vendl and Holzinger that was outlined in Section 3.1 [11]. This metric forms our "standard" cost function that solely considers the detection capabilities of an architecture for cislunar surveillance:

$$J_S(\mathbf{C}_N) = \min_{\mathbf{C}_N} \left(-\Gamma_v\right) \ , \tag{24}$$

where the vector $\mathbf{C}_N$ is an $(N \times 3)$ surveillance network vector consisting of the observer parameters of N different constituent spacecraft ($\mathbf{c}_i$ for $i \in [1, N]$) that make up the candidate surveillance network:

$$\mathbf{C}_N = [\mathbf{c}_0, \mathbf{c}_1, \ldots, \mathbf{c}_N] \ , \tag{25}$$

and the constituent spacecraft are defined by a cislunar orbital family, a period within that family (P_i), and the relative initial phasing offset of the observer from the initial state vector (ϑ_i) [5]:

$$\mathbf{c}_i = (\text{Family}_i, P_i, \vartheta_i) \ , \tag{26}$$

While the standard cost function of Equation 24 is useful for comparing the relative detection capability of different architectures, it does not capture any information about operational cost factors. For example, if the ΔV required for station-keeping in an orbital slot with high detection performance is prohibitive, then the recommendations of architectures derived using Equation 24 may not be not useful for operational planning [3]. In order to account for this potential discrepancy, we augment the "standard" cost function with "operational" cost and performance metrics as outlined in Sections 3.3 to 3.2. This new cost function is then represented as:

$$J_{S+O}(\mathbf{C}_N) = \min_{\mathbf{C}_N} \left(-\bar{\Gamma}_v, \bar{\sigma}, \bar{\kappa}, \right) \tag{27}$$

where $\bar{\Gamma}_v$ is observer-averaged visibility metric of the candidate surveillance network (Section 3.1), $\bar{\sigma}$ is the observer-averaged stability metric for the candidate constellation (Section 3.2), and $\bar{\kappa}$ is observer-averaged logarithm of the condition number of the observability Gramian for horizon-based optical navigation (Section 3.3). Our novel optimization metric of Equation 27 represents an approach which is tailored to consider the operational challenges of deploying and maintaining distributed sensors within the challenging cislunar volume. Additionally, it considers the optical navigation derived uncertainty in an observer's estimated position in the form of $\bar{\kappa}$, which can influence both network maintenance and orbit determination solutions.

Both the standard cost function (Equation 24) and the operational cost function (Equation 27) were optimized over a range of potential observer combinations. Table 1 details the full search space of potential values for usage in Equation 26. There were in total 7 different cislunar families considered for optimization of surveillance of the cislunar highway. The range of potential periods (P_i) for each family varied according to the achievable range under the CR3BP dynamics. Additionally, the initial phasing of each candidate orbit (ϑ_i) was allowed to vary discretely in order to achieve the appropriate solar phase angle conditions to maximize observability of the targets that were distributed along the cislunar highway. In order to vary this initial phasing, we performed the operations on the initial state vector of each candidate orbit according to the rotation operation outlined by Vendl and Holzinger [11].

4.2 Multi-Disciplinary Analysis and Optimization (MDAO)

The cislunar dynamics propagator (Section 2), the cost models of interest (Section 4.1), and the simulation design space (Section 5) were all integrated into a unified modeling environment using a custom Python-based Multi-Disciplinary Analysis and Optimization (MDAO) framework. Models and costs metrics are integrated into the environment via wrapper scripts that translate codes for engineering analysis from their native language (i.e. Matlab, Python, Julia, etc.) into standardized interfaces that can be interpreted by a common data parser. These standardized models are then packaged into a library and loaded into the modeling environment at runtime based on a user-defined configuration. Loaded models are compiled into modeling environment based on National Aeronautics and Space Administration's (NASA) open-source OpenMDAO Python package [26]. This approach allows the modeling environment to be rapidly

Table 1: Orbital families considered for optimization of the distributed cislunar surveillance network in this study.

Family ID	Family	Period Range (days)	ϑ [Min, Max] (degrees)
1	L1 Lyapunov	11.93 - 33.00	0°, 360°
2	L2 Lyapunov	14.95 - 36.41	0°, 360°
3	L1 Northern Halo	7.99 - 13.84	0°, 360°
4	L2 Northern Halo	3.18 - 15.14	0°, 360°
5	L1 Southern Halo	7.99 - 13.84	0°, 360°
6	L2 Southern Halo	3.18 - 15.14	0°, 360°
7	Distant Retrograde Orbit (DRO)	1.81 - 27.95	0°, 360°

configurable and highly customizable. A diagram of the workflow of the MDAO framework that is leveraged for this study is shown in Figure 4.

As shown in Figure 4, each model and its associated wrapper are bundled into modules and packaged within a unified library ("Model Library"). All desired models for a design reference mission can then be individually loaded and compiled into a modeling environment at runtime ("Model Loader"). This modularization allows a user to quickly setup different cost functions (i.e. Equation 24 vs. Equation 27) with minimal additional coding input. This is made possible by OpenMDAO's powerful data management tools. Once each model has been loaded into the environment OpenMDAO fully connects each model, such as the Christian-Robinson optical navigation algorithm (Section 3.3) and the cislunar dynamics propagator (Section 2), and manages the flow of data between them. As OpenMDAO receives information from the various models and cost functions, OpenMDAO's built-in optimization drivers ("OpenMDAO Solver") iteratively solve for ideal solutions to the specified cost function and outputs the final result to the user for further analysis ("Data Writer").

The simple genetic algorithm (*"SimpleGADriver"*) optimization driver built into OpenMDAO was chosen as the solver for this analysis, in part due to its support for multi-objective optimization, and both constrained and unconstrained cost functions [27]. A detailed discussion of genetic algorithms can be found in many different sources (i.e. [28]), therefore only a brief overview will be discussed here. In general, a genetic algorithm attempts to replicate the evolutionary processes found in nature to identify optimal solutions to engineering problems. The value of each design variable is decomposed into a series of binary bits which function as genes. At the initial epoch, a set of cases (i.e. "population") is generated wherein each member contains a randomly generated set of genes to be evolved over the course of the simulation. At the end of each epoch, each member of the population is evaluated using the modeling environment to determine the system's response as given by the cost function. This response is then used to rank each member of the population: members of the population with the largest cost response are eliminated from the population, while those with the smallest cost are used to seed the population of the next generation. The evolutionary epoch cycle is repeated until the cost of each subsequent generation fails to sufficiently improve on the cost of the previous generation [28].

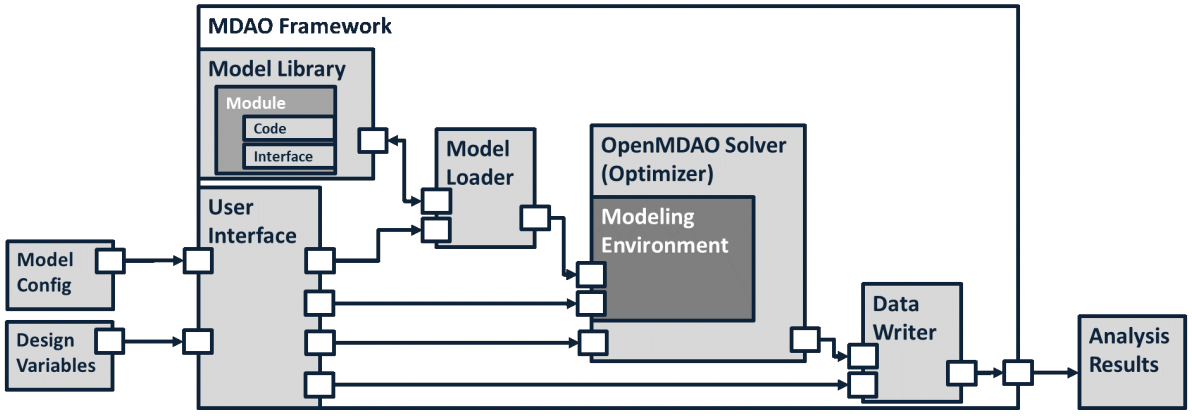

Fig. 4: The Multi-Disciplinary Analysis and Optimization (MDAO) framework created for optimization of custom cislunar Space Domain Awareness (SDA) design problems and cost objectives.

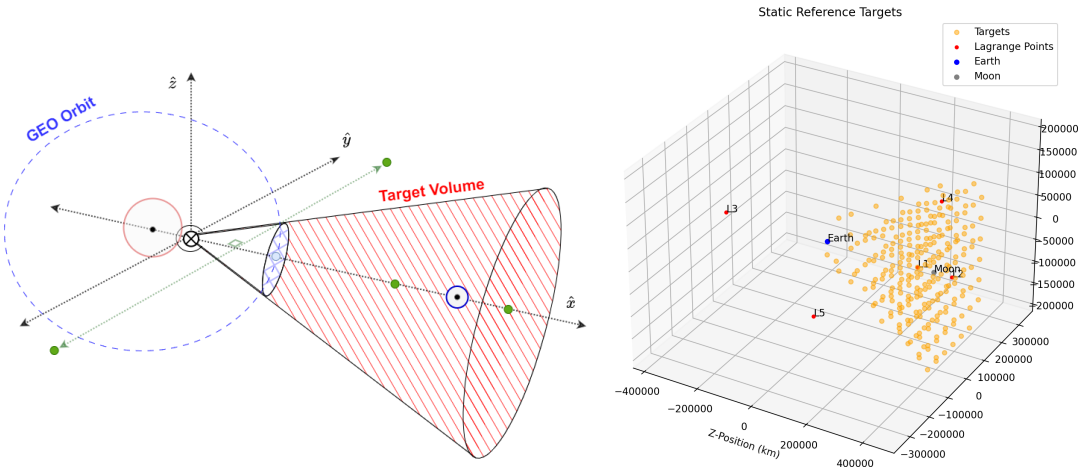

Fig. 5: Diagram outlining the geometry of the target volume of interest (left) and the equidistant targets spaced throughout this volume in the MDAO simulation (right).

There are several advantages to leveraging genetic evolutionary algorithms over other optimization drivers. Because genetic algorithms are non-gradient based methods, and they are more robust to irregular or discontinuous design spaces. Additionally, genetic algorithms do not require a scalar objective function meaning that they can be used to identify multi-dimensional pareto fronts. Finally, genetic algorithms are easily parallelizable due to each member of a given population being independently evaluated within each epoch. One notable downside of genetic algorithms, however, is that they can potentially take slower and more irregular paths towards optimal solutions to a cost function due to their reliance on random evolution of populations across epochs [28, 27].

While the "standard" cost function of Equation 24 is a scalar, the proposed "operational" cost function of Equation 27 is multi-dimensional. While it is possible to create a weighting function to convert the cost vector of Equation 27 into a scalar objective function to identify a single ideal solution, this approach would limit design space visibility. Instead of trying to identify a single solution which minimized all of the cost criteria, the optimization driver was used to identify the set of solutions which each minimize some portion of the cost criteria, known as the "Pareto Front." The "Pareto Front" is composed of design solutions which are non-dominated, meaning they minimize at least one cost metric more than any other solution. Using this approach, it is possible to identify how changing the weight of each cost metric alters the ideal solution in a post-optimization qualitative analysis [29].

5. SIMULATION SETUP

Our goal in this study is the optimize the capability of a surveillance satellite to monitor the cislunar volume over time. We therefore evaluate sensor detection performance when targeting a volume covering an approximately 25° solid angle extending from from the geostationary (GEO) belt out to the Earth-Moon L2 point. This choice is motivated by previous optimization studies [11, 5] that consider this region to be of high interest due to the high volume of Moon-bound traffic that will traverse this region and the limited ability for Earth-based telescopes to adequately surveil the region due to lunar brightness drowning out satellite signatures [2]. Targets were distributed in an equidistant manner across this truncated cone of interest, and each of the considered distributed space-based sensors computed the apparent visual magnitude of each target at every timestep for the duration of the simulation. A diagram of the distribution of the targets within the rotating frame is shown in Figure 5. The targets were assumed to have reflectance properties ($\rho_s = 0$, $\rho_d = 0.2$) and a diameter of d_T = 1 meter. The telescope that was attempting to detect these objects was taken to have a apparent magnitude cutoff $m_{co} = 18$, and we set the requirement that it detected objects with this apparent magnitude for $\alpha = 85\%$ of the duration of the simulation.

Along with the target and telescope properties, the orientation of incident solar radiation relative to the rotating frame is a critical quality for determining observablity according to the solar phase angle term of Equation 14. In this work, the solar direction is defined relative to an arbitrarily chosen initial reference epoch for the solar position at initial

Table 2: Table of simulation parameters used to generate the multi-objective optimization cost functions in this study.

Parameter	Unit	Value
Initial Epoch (t_0)	Time and Date	2022 JAN 01 00:00:00.000
Campaign Duration (ΔT)	Days	365
Time Step	Seconds	1440
Number of Targets	-	259
Target Diameter (d_T)	Meters	1
Target Specular Reflectance (ρ_s)	-	0.0
Target Diffuse Reflectance (ρ_d)	-	0.2
Cutoff Apparent Magnitude (m_{co})	-	18
Fraction of Time Visible Requirement (α)	%	85
Offset for Condition Number in Position (δ_p)	-	0.001
Offset for Condition Number in Velocity (δ_v)	-	$2\pi(0.001)$/ P
Number of Spacecraft (N)	-	3, 5, 7

time (t_0). The initial epoch time for our study was chosen to be equal to a value of t_0='2024 JAN 01 00:00:00.000'. The JPL NAIF SPICE data is then used to obtain the vector from the Earth-Moon barycenter to the Sun at all times relative to this initial epoch ($t - t_0$). For all simulations, the Sun-direction vector is extracted at each time step where the observation is to be simulated over the duration of the simulation ΔT = 365 days, based on the assumption that one year is a sufficiently long period of time to produce a generalized result for seeing all potential solar geometries relative to the ecliptic plane [3].

The simulation properties for the targets, detectors, and the solar conditions is shown in Table 2. These simulation parameters were used to optimize the two different cost functions provided in Equations 24 and 27, with the results over these simulation parameters presented in Section 6.

6. RESULTS

6.1 Single-Objective Optimization: Maximizing Percentage Search Volume Visible over Time

We first optimize the genetic algorithm over the orbital Families from Table 1 using the simulation parameters in Table 2 for the cost function in Equation 24. This optimization result represents the current approach in the SDA community in which we only optimize the percentage of the search volume that is visible over time without consideration of the potential complexities with preserving the constellation for long durations. As was discussed in Table 2, this was performed for three different numbers of spacecraft (N): 3, 5, and 7.

Because only a single parameter was considered for the MDAO optimization on the cost function of Equation 24, we plot these results in the form of bar charts rather than a pareto front. Figures 6 (a)-(c) show the maximum Γ_v values for cases that survived all evolutionary cycles of the genetic MDAO optimizer. Each bar chart is segmented along the x-axis by the number of unique observers that comprised each of the cases. This discrete segmentation of the cases by number of unique families in the surviving constellation is meant to reveal insight on the the angular and geometric diversity of constellations in the surviving cases from the evolutionary cycles.

For the case of N=3 observer constellations, Figure 6 (a) highlights that augmenting a surveillance constellation with just a second unique cislunar family can improve the constellation's ability to maintain low standoff distances with a larger proportion of the target cislunar volume across time. As will be shown, the optimal constellation for $N = 3$ satellites in Figure 7 reveals that in order to maximize the percentage of time that the cislunar highway is visible, the surveillance orbits should be centered about diverse equilibrium points of the Earth-Moon rotating frame such as the Moon and the Earth-Moon Lagrange $L1$ point [3]. The benefits of distributed observer diversity in both equilibrium point and angular distribution can be used to explain the jump in average visibility when going from just a single unique cislunar family ($\Gamma_v = 0.645$) to two unique cislunar families ($\Gamma_v = 0.78$) for the $N = 3$ case in Figure 6 (a).

These results generally hold with some exceptions when the optimizer was allowed to consider $N = 5$ and $N = 7$ spacecraft for the constellation as is seen in Figures 6 (b) and (c), respectively. One exception that can be seen in Fig-

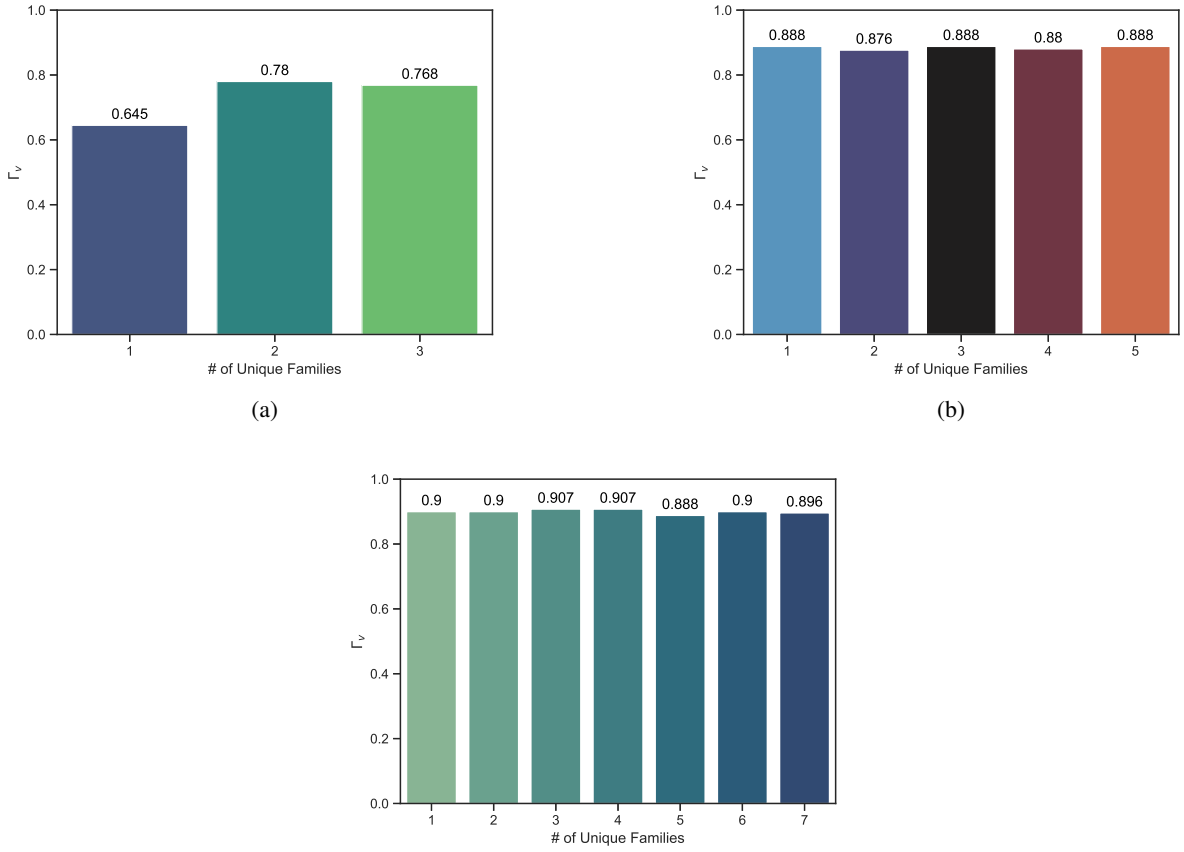

Fig. 6: The maximum Γ_v values resulting from the MDAO genetic algorithm optimization of Equation 24 for the case of a constellation of (a) N=3, (b) N=5, and (c) N=7 satellites.

ure 6 (b) is that there is a negligible increase in Γ_v when going from just a single unique cislunar family ($\Gamma_v = 0.8881$) to five unique cislunar families ($\Gamma_v = 0.8884$) for constellations consisting of $N = 5$ surveillance assets. This result is slightly misleading, as the diversity is occurring across period and phase within a single cislunar family. As will be shown later, surveillance constellations consisting solely of the Distant Retrograde Orbit (DRO) family provided high levels of observability of up to $\Gamma_v \approx 0.89$ when the assets were dispersed across the full period range considered in Table 1 and at the same time were properly phased to overcome exclusion zones pointing towards the sun, earth, and moon. This trend can also be seen for the $N = 7$ results in Figure 6 (c), where the single unique family case has a nearly equal Γ_v value to the seven unique family case. However, we note that the optimum solution for the $N = 7$ constellation occurs when four unique cislunar families are considered in the sureveillance constellation, providing evidence that cislunar orbit and equilibrium point diversity can improve custody maintenance. In summary, we believe that the distribution of MDAO optimization results in Figures 6 (a) through (c) confirm previous findings that angular, geometric, and phasing diversity across a surveillance constellation critical to optimizing cislunar surveillance performance [3, 5, 7, 9].

The parameters of the global optimum constellations for the values of N considered when performing genetic algorithm optimization using the cost function of Equation 24 are shown in Table 3. Additionally, we provide plots of the trajectories for these parameters when plotted over a single period in Figure 7. These results were generated without consideration of any operational cost factors, which were incorporated into the optimization process to produce the results shown in the next section.

For the $N = 3$ case, the optimal surveillance constellation consists of two unique cislunar families: the DRO family,

Table 3: Orbital parameters for the optimal constellations when using the standard cost function of Equation 24 in the MDAO genetic algorithm optimizer.

N	Γ_v	Orbit Family	Orbit ID	Orbital Period (days)	ϑ (degrees)
3	0.7799	DRO	7	15.253	242.824
		L1 Lyapunov	1	29.549	131.412
		DRO	7	13.490	1.412
5	0.8880	DRO	7	21.423	135.529
		DRO	7	22.011	104.471
		DRO	7	22.794	232.941
		DRO	7	21.913	331.765
		DRO	7	22.305	271.059
7	0.9073	DRO	7	22.990	227.294
		DRO	7	14.567	208.941
		L1 Halo Southern	5	10.771	295.059
		DRO	7	13.294	24.000
		DRO	7	18.779	230.113
		L1 Lyapunov	1	30.195	152.471
		L1 Halo Southern	5	10.565	304.941

and a Lyapunov orbit centered about the $L1$ equilibrium point. We note that the genetic algorithm optimizer chose the DRO orbits that are approximately of the same period, but that differ in angles by greater than 180° in phase. This makes intuitive sense, as one DRO observer can always maintain an appropriate solar phasing with respect to the frustum of interest, as has been shown in previous studies [5, 11].

For the $N = 5$ case, the genetic algorithm optimizer chose a constellation consisting of only DRO orbiters in order to maximize Γ_v. The optimizer also identified other, more diverse constellations, that had very similar values of Γ_v, however, the DRO-only constellation had the highest performance. This suggests that the Γ_v metric is multi-polar with respect orbit family selection, meaning there are multiple architectures that produce local maxima in terms of Γ_v. Considering Γ_v as the only performance metric it is not possible to distinguish between each maximum without considering other factors.

For the $N = 7$ case, there were three unique families in the optimal constellation, an increase in the number of unique cislunar families relative to the $N = 5$ case that was just discussed. Like in the $N = 5$ case, the DRO family that can be considered in-plane (i.e. of higher expected stability) featured prominently in this optimal result despite the fact that the optimizer did not consider stability or navigation cost factors when arriving at the optimal constellations of Table 3. This suggests that the DRO family can provide high visibility performance on the cislunar volume of interest if the observers have sufficient diversity in phasing and period, as in the case of the three constituent DRO satellites in Figure 7 (c). A second observation that can be noted for the $N = 7$ case is that there are two out-of-plane *L1* Halo Southern orbits in the optimal $N = 7$ constellation of Figure 7 (c). Table 3 reveals that these two orbits have nearly identical phasing and periods, suggesting that they may provide nearly identical visibility into the frustum of interest over time. This suggests that there may be a saturation in the visibility performance that can be obtained for $N \geq 5$ observers for the volume of interest in Figure 5 and simulation parameters of Table 2, which is supported by the bar charts in Figure 6 (b) and (c).

6.2 Multi-objective optimization: Incorporation of Operational Cost Functions

The optimal constellations for various N values in Figure 7 and Table 3 were arrived at by only considering the visibility performance of the constellation over time via Equation 24. As was discussed in Section 3, Equation 24 does not consider the cost factors associated with navigating individual satellites and maintaining them in their nominal orbits via stationkeeping maneuvers over time. In order to explicitly incorporate these factors into the genetic algorithm optimization, we developed a multi-objective optimization formulation with the cost metrics in Equation 27. This equation has cost factors that approximate the costs of performing stationkeeping and horizon-based optical navigation over the duration of the mission.

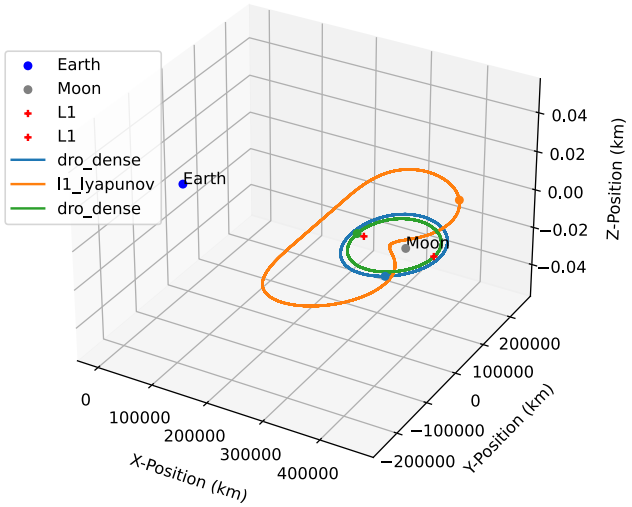

(a)

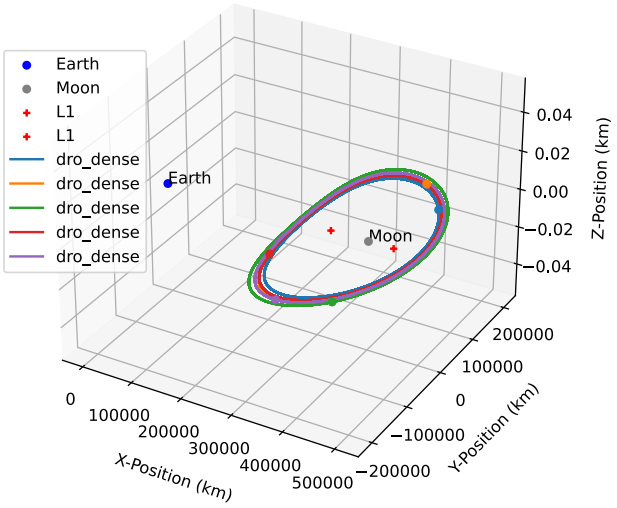

(b)

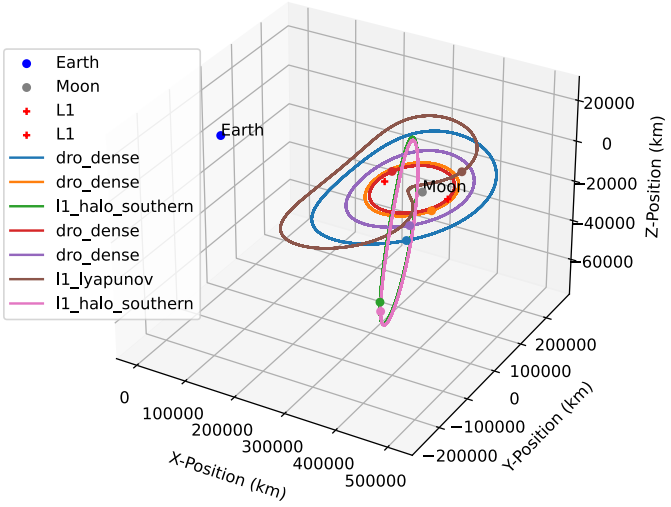

(c)

Fig. 7: Optimal constellations when using the standard cost function of Equation 24 in the MDAO genetic algorithm optimizer for the case of (a) $N = 2$, (b) $N = 5$, and (c) $N = 7$ observers in the constellation.

Table 4: Orbital parameters for the optimal constellations when using the operational cost function of Equation 27 in the MDAO genetic algorithm optimizer.

N	Γ_v	Orbit Family	Orbit ID	Orbital Period (days)	ϑ (degrees)
3	0.5714	DRO	7	15.253	242.824
		DRO	7	29.549	121.412
		DRO	7	13.490	1.412
5	0.8880	DRO	7	21.423	135.529
		DRO	7	22.011	104.471
		DRO	7	22.794	232.941
		DRO	7	21.913	331.765
		DRO	7	22.305	271.059
7	0.8996	DRO	7	22.990	227.294
		DRO	7	14.567	208.941
		DRO	7	10.771	295.059
		DRO	7	13.294	24.000
		DRO	7	18.779	230.118
		DRO	7	30.195	152.471
		DRO	7	10.565	304.941

To evaluate one example of the Pareto optimal solution, we convert this equation into a single-objective optimization by assigning the weights to each objective. In this initial study, we chose to assign $1/2$ to the visibility metric, and $1/4$ each to the remaining metrics; however, we note that the weighting can be rapidly adjusted and the simulation re-run due to the configurable MDAO framework that was presented in Section 4. Using this weighted cost function in the genetic algorithm optimizer led to the "operationally informed" optimal constellations in Figure 8 and Table 4. One point that immediately becomes apparent from this result is that the optimizer has minimized the weighted cost function by forming constellations consisting solely of the DRO family for the $N = 3$, $N = 5$, and $N = 7$ simulations. For example, for the $N = 3$ problem the use of Equation 27 as opposed to Equation 24 has led to a family consisting of three DRO observers in Figure 8 (a) as opposed to the two DRO observers that comprised the optimal orbit of Figure 7 (a). In other words, the optimizer exchanged an $L1$ Lyapunov observer for an additional DRO observer, which led to a nearly 27% decrease in visibility performance from a value of $\Gamma_v = 0.7799$ (Table 3 for $N = 3$) to $\Gamma_v = 0.571$ (Table 4 for $N = 3$). The Lyapunov observer that was substituted had a stability index on the order of approximately $\sigma \approx 50$, while the DRO observer had a stability index of approximately $\sigma \approx 1$. Because both of these stability indices are relatively small relative to the ranges of σ considered, it can be argued that the degradation in visibility performance is not worth the increase in the average stability of the constellation. On the other hand, the $N = 5$ and $N = 7$ results that were derived using the operationally informed cost objective provide greatly improved visibility performance relative to the $N = 3$ case, with $\Gamma_v = 0.888$ and $\Gamma_v = 0.900$ given in Table 4 for the $N = 5$ and $N = 7$ cases, respectively. Furthermore, the difference in Γ_v between the standard and operational objective functions was very small for both of these cases. For the $N = 5$ case, the same constellation was found to be optimal for both the standard and operational objective functions. For the $N = 7$ case there was a small decrease in Γ_v equal to approximately 0.8%. This reinforces the advantages of the MDAO approach that considers both performance and cost metrics. For a significant change in architecture, but only minimal change in observation performance there is a large reduction in constellation cost. This approach also allowed for differentiation between the multiple maxima in terms of Γ_v that were identified in the $N = 5$ case using the standard objective function.

It must be noted that the result of Table 4 was derived using a fixed weighting of the performance metrics considered in Equation 27. Different combinations of the scalar weightings can lead to very different global "optimum" solutions, with some of them providing visibility performance on the same level as solutions derived using the visibility cost function of Equation 24. In order to see this, we can analyze the Pareto front of cases provided at the end of the MDAO genetic algorithm optimizer's evolutionary cycles.

The Pareto front of optimal solutions derived by considering the operational cost function of Equation 27 is shown along a slice of the 3-dimensional parameter plane in Figure 9. One thing that becomes apparent from this plot is that

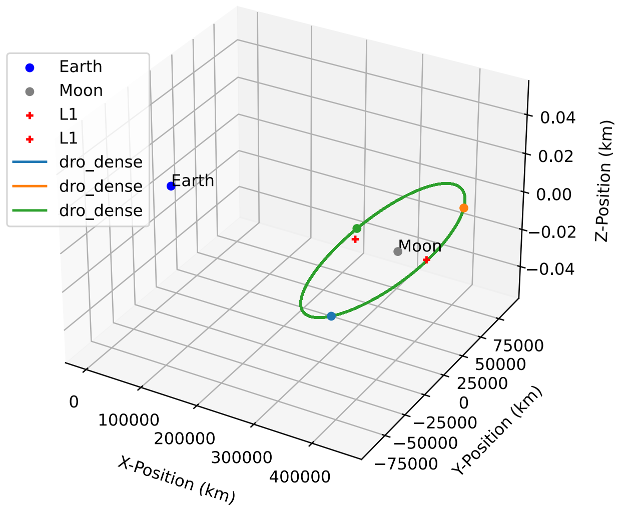

(a)

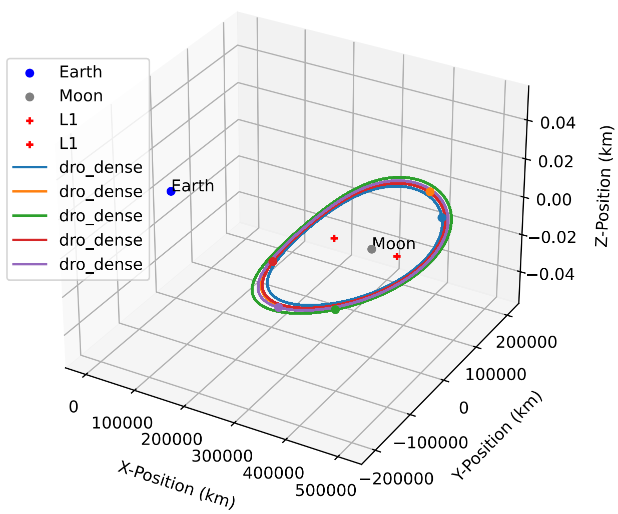

(b)

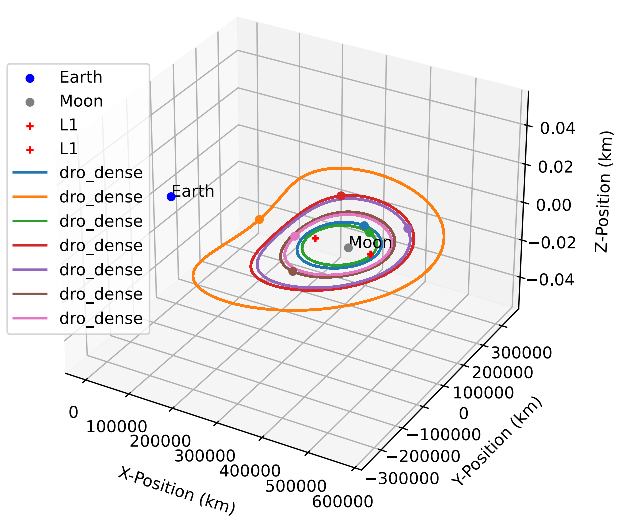
Earth
Moon
L1
L1
dro_dense
dro_dense
dro_dense
dro_dense
dro_dense
dro_dense
dro_dense
Earth
Moon
X-Position (km)
Y-Position (km)
Z-Position (km)
0
100000
200000
300000
400000
500000
600000
−300000
−200000
−100000
0
100000
200000
300000
0.04
0.02
0.00
−0.02
−0.04

(c)

Fig. 8: Optimal constellations when using the operational factors cost function of Equation 27 in the MDAO genetic algorithm optimizer for the case of (a) $N = 3$, (b) $N = 5$, and (c) $N = 7$ observers in the constellation.

the average stability index ($\bar{\sigma}$) compresses information along the $\bar{\sigma} \approx 1$ vertical line. This can be explained by the observation that DRO orbiters for the period range considered in this study (see Table 1) all possess stability indices on the order of $\sigma \approx 1$ [30]. Therefore, the optimizer is able to trivially minimize the Pareto front along the $\bar{\sigma}$ by simply including DRO observers in the solution. Indeed, the vast majority of cases on the Pareto fronts of Figure 9 across all values of N solely include one unique family: the DRO. This result leads us to believe that while the stability index has been suggested as a potential optimization metric in previous studies [11, 5], it possesses limited utility due to the trivial nature of minimizing it by restricting the constellation satellites to those families with primary bodies (i.e. the Moon) as their equilibrium point. As an alternative, we believe that metrics that account for stationkeeping costs in the form of ΔV [7] or rates of departure from a nominal orbit [19] are more useful for deriving operationally useful cislunar surveillance orbits. It is also important to note that the final solution depends on the weighting among each cost metric; thus, the selection of a Pareto-optimal solution that meets several mission requirements needs to have a human-in-the-loop analysis in order to overrule solutions that do not meet the primary mission objective of surveilling the cislunar volume for long durations of time.

7. CONCLUSIONS

In this paper, we developed a rapidly configurable MDAO framework for designing cislunar surveillance constellations. In the developed MDAO framework, the variables include the orbits of each observing satellite in the constellation, and the objectives include not only the coverage performance metric but also the operational cost metrics including the orbital stability and the navigational uncertainty. This integrated framework enables the mission designer to trade off the performance and the cost to identify the Pareto optimal solutions. The analysis results demonstrated the effectiveness and limits of the proposed multi-objective MDAO analysis. Specifically, the global optimum solution derived using our chosen set of performance-to-cost weightings across the three considered metrics had a bias towards selecting Distant Retrograde Orbiters (DROs) due to the high levels of stability that accompany their orbit about the Moon within the plane of the Earth-Moon rotating system. This bias towards selecting DROs leads to sub-optimal visibility performance relative to the maximum possible achievable level of the Pareto front solutions. Despite the genetic optimizer's bias towards *in-plane* orbiters, however, the optimizer of the MDAO system was able to produce constellations that nearly matched the visibility performance of solutions derived by solely considering the visibility metric. Specifically, for the $N = 7$ observer optimization case, it was found that incorporation of operational cost factors only yielded a decrease in detectability performance of only 0.8%.

As part of future work, we plan to consider a more diverse set of operational cost metrics; particularly, the stability index used in this paper does not provide accurate information about the ΔV needed for stationkeeping and can be trivially minimized by selecting Distant Retrograde Orbiters (DROs) that have a nearly constant stability index of ≈ 1. We therefore suggest that stability indices be replaced with other more operationally relevant metrics, despite their usage in previous studies to represent stationkeeping costs [5, 11]. Furthermore, a more in-depth orbital determination model can be incorporated as a performance evaluation model beyond the visibility metric used in this paper.

8. REFERENCES

[1] Northern Sky Research (NSR). Moon market analysis, 2nd edition. *https://www.nsr.com/?research= moon-market-analysis-2nd-edition*.

[2] MJ Holzinger, CC Chow, and P Garretson. *A primer on cislunar space*. Air Force Research Laboratory, 2021.

[3] Erin E Fowler and Derek A Paley. Observability metrics for space-based cislunar domain awareness. *The Journal of the Astronautical Sciences*, 70(2):10, 2023.

[4] Carolin Frueh, Kathleen Howell, Kyle J DeMars, and Surabhi Bhadauria. Cislunar space situational awareness. In *31st AIAA/AAS Space Flight Mechanics Meeting*, pages 6–7, 2021.

[5] Lois Visonneau, Yuri Shimane, and Koki Ho. Optimizing multi-spacecraft cislunar space domain awareness systems via hidden-genes genetic algorithm. *The Journal of the Astronautical Sciences*, 70(22), 2023.

[6] E.J. Felt. Development corps overview: Space vehicles directorate. *Air Force Research Laboratory (AFRL)*, 2020.

[7] Erin E Fowler, Stella B Hurtt, and Derek A Paley. Orbit design for cislunar space domain awareness. In *2nd IAA Conference on Space Situational Awareness (ICSSA), Washington, District of Columbia*, 2020.

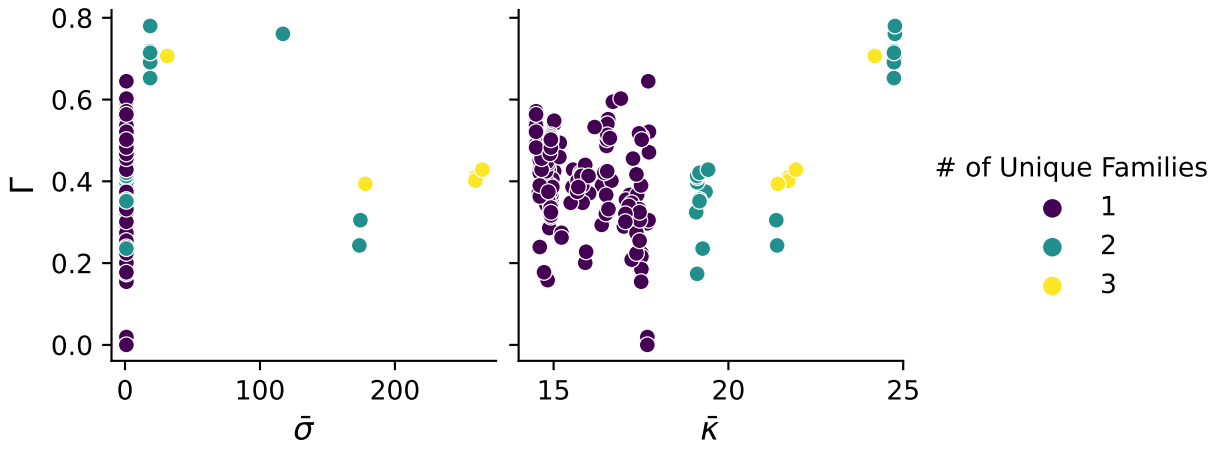

(a)

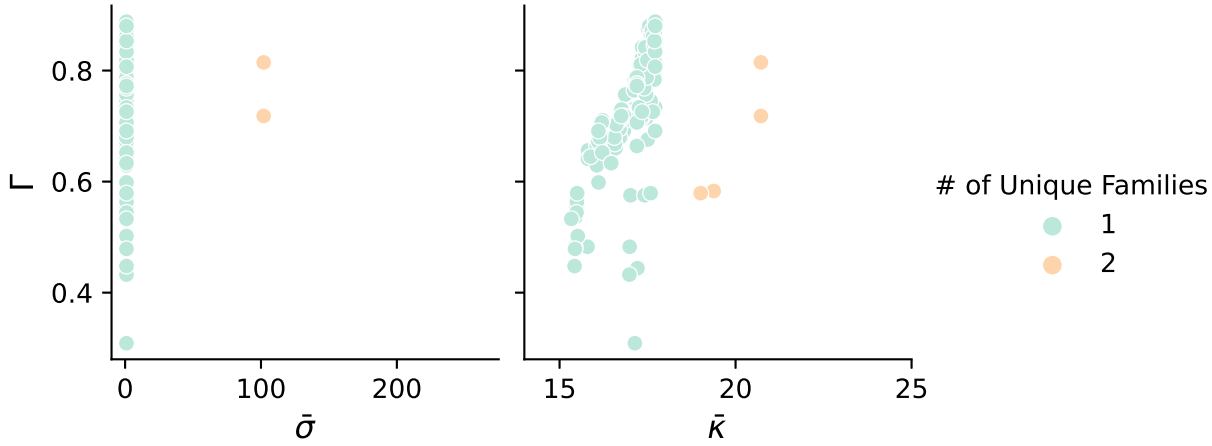

(b)

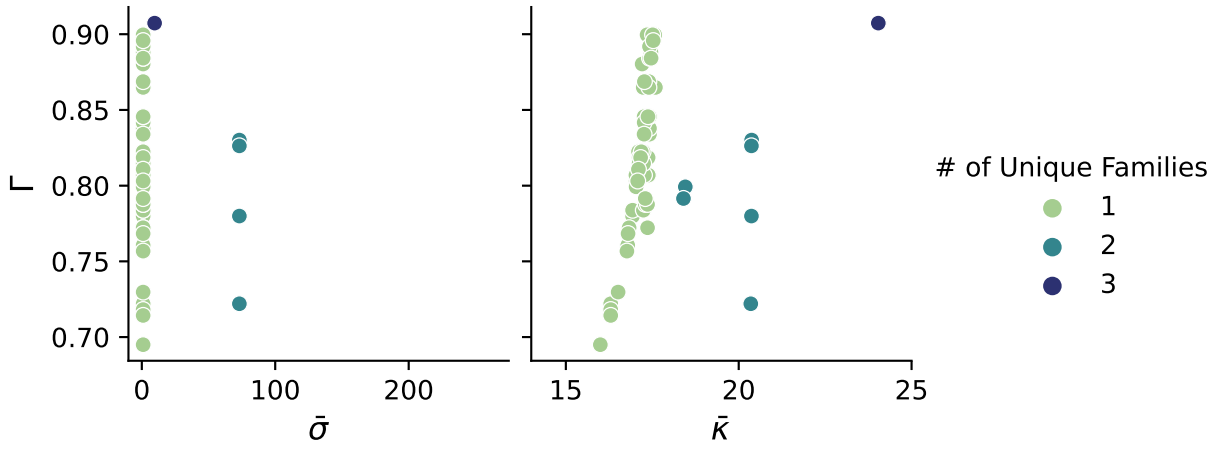

(c)

Fig. 9: Representation of a cross section of the 3-dimensional pareto front resulting from the use of Equation 27 in the MDAO genetic algorithm optimizer for the case of (a) N =3, (b) N =5, and (c) N =7 observers in the cislunar surveillance constellation.

[8] Surabhi Bhadauria and Carolin Frueh. Optical observation regions in cislunar space using the bi-circular restricted four body problem geometry. *Advanced Maui Optical and Space Surveillance Technologies Conference*, 2022.

[9] Gregory Badura, Yuri Shimane, Alaric Gregoire, Rohan Patel, Matthew Gilmartin, Kunal Gangolli, Lois Visonneau, Joshua Tysor, Saikrishna Manojkumar, Francis Humphrey, Chris Valenta1, Reilly Blair1, Nelson Lourenco1, Jason Hodkin, Alicia Sudol, Mariel Borowitz, Brian Gunter, John Christian, and Koki Ho. System design and analysis for cislunar space domain awareness through distributed sensors. In *AAS/AIAA Astrodynamics Specialist Conference, Charlotte, NC*, pages 1–20, 2022.

[10] Simon R Knister. Evaluation framework for cislunar space domain awareness (sda) systems. 2020.

[11] Jacob K Vendl and Marcus J Holzinger. Cislunar periodic orbit analysis for persistent space object detection capability. *Journal of Spacecraft and Rockets*, 58(4):1174–1185, 2021.

[12] Wang Sang Koon, Martin W Lo, Jerrold E Marsden, and Shane D Ross. Dynamical systems, the three-body problem and space mission design. In *Equadiff 99: (In 2 Volumes)*, pages 1167–1181. World Scientific, 2000.

[13] John Danby. Fundamentals of celestial mechanics. *Richmond: Willman-Bell*, 1992.

[14] Archie E Roy. *Orbital motion*. CRC Press, 2020.

[15] R Coder and M Holzinger. Sizing of a raven-class telescope using performance sensitivities. In *Advanced Maui Optical and Space Surveillance Technologies Conference*, page E28, 2013.

[16] Bruce Hapke. Bidirectional reflectance spectroscopy: 1. theory. *Journal of Geophysical Research: Solid Earth*, 86(B4):3039–3054, 1981.

[17] Davide Guzzetti, Emily M Zimovan, Kathleen C Howell, and Diane C Davis. Stationkeeping analysis for spacecraft in lunar near rectilinear halo orbits. In *27th AAS/AIAA Space Flight Mechanics Meeting*, volume 160, pages 3199–3218. American Astronautical Society San Antonio, Texas, 2017.

[18] Samuel Wishnek, Marcus J Holzinger, and Patrick Handley. Robust cislunar initial orbit determination. In *AMOS Conf. Proc*, 2021.

[19] Diane Davis, Sagar Bhatt, Kathleen Howell, Jiann-Woei Jang, Ryan Whitley, Fred Clark, Davide Guzzetti, Emily Zimovan, and Gregg Barton. Orbit maintenance and navigation of human spacecraft at cislunar near rectilinear halo orbits. In *AAS/AIAA Space Flight Mechanics Meeting*, number JSC-CN-38626, 2017.

[20] Adam P Wilmer. Space domain awareness assessment of cislunar periodic orbits for lagrange point surveillance. 2021.

[21] Arthur J Krener and Kayo Ide. Measures of unobservability. In *Proceedings of the 48h IEEE Conference on Decision and Control (CDC) held jointly with 2009 28th Chinese Control Conference*, pages 6401–6406. IEEE, 2009.

[22] Richard Luquette and Robert Sanner. Linear state-space representation of the dynamics of relative motion, based on restricted three body dynamics. In *AIAA Guidance, Navigation, and Control Conference and Exhibit*, page 4783, 2004.

[23] John A Christian. A tutorial on horizon-based optical navigation and attitude determination with space imaging systems. *IEEE Access*, 9:19819–19853, 2021.

[24] John A Christian. Accurate planetary limb localization for image-based spacecraft navigation. *Journal of Spacecraft and Rockets*, 54(3):708–730, 2017.

[25] Devin T Renshaw and John A Christian. Subpixel localization of isolated edges and streaks in digital images. *Journal of Imaging*, 6(5):33, 2020.

[26] Justin Gray, Kenneth Moore, and Bret Naylor. Openmdao: An open source framework for multidisciplinary analysis and optimization. In *13th AIAA/ISSMO Multidisciplinary Analysis Optimization Conference*, page 9101, 2010.

[27] Brian R Jones, William A Crossley, and Anastasios S Lyrintzis. Aerodynamic and aeroacoustic optimization of rotorcraft airfoils via a parallel genetic algorithm. *Journal of aircraft*, 37(6):1088–1096, 2000.

[28] Matthew P Ferringer, Ronald S Clifton, and Timothy G Thompson. Efficient and accurate evolutionary multi-objective optimization paradigms for satellite constellation design. *Journal of Spacecraft and Rockets*, 44(3):682–691, 2007.

[29] Albert R Vasso, Richard G Cobb, John M Colombi, Bryan D Little, and David W Meyer. Multi-day evaluation of space domain awareness architectures via decision analysis and multi-objective optimization. *The Journal of Defense Modeling and Simulation*, page 15485129211067767, 2022.

[30] Mar Vaquero and Juan Senent. Poincaré: A multi-body, multi-system trajectory design tool. 2018.